Arabian Journal of Geosciences (2023) 16:482
https://doi.org/10.1007/s12517-023-11597-6

TECHNICAL NOTE

Simulations on time-dependent behaviour based on wall deflection of deep excavations in Jakarta

Fuchen Teng[1] · Bin-Chen Benson Hsiung[2] · Muhammad Dwiyanto Agung Prakasa[3] · Kuo-Hsin Yang[4] · Anthony[1] · Richard Litanes[5]

Received: 6 February 2023 / Accepted: 13 July 2023 / Published online: 21 July 2023

Abstract

Finite element analyses were conducted on two prominent cases of large-scale deep excavation in Central Jakarta, Indonesia. Large lateral wall deflections were observed during the final excavation stage, presumably due to clay's time-dependent behaviour, for example, creep and consolidation (i.e., the excess pore water pressure being dissipated). Three-dimensional numerical analyses were executed using the soft-soil and soft-soil-creep models, which are advanced soil models, under the consideration of time-dependent effects. This study discovered that the time-dependent characteristics of clay in Central Jakarta contributed 23%–26% of the total wall deflection. Both soil creep and consolidation played a role in the major wall deformation in the final stage, and consolidation caused by the excavation had a stronger impact on wall deformation than did soil creep, with the impact being affected by the excavation area size, soft clay layer thickness, and presence of permeable materials (such as sand lenses).

Keywords Deep excavation · Time-dependent behaviour of clays · Central Jakarta · Three-dimensional numerical simulation · Wall deflection · Presence of permeable materials

Introduction

Indonesia's capital Jakarta is undergoing rapid development and construction. Transportation services for its 10 million residents are currently limited, and to expand the transportation network, additional underground space is needed. Many underground construction projects involving deep excavation have thus been implemented recently. Scholars have reported on how deep excavation has induced wall behaviour in many underground construction projects worldwide (Clough and O'Rourke 1990; Ou et al. 1996, 1998; Ou 2006; Finno et al. 2015; Dong et al. 2017; Hsiung et al. 2018). There are many factors may affect the deformation of deep excavation as stated by Peck (Peck 1969) such as excavation depth, soil type/strength, stiffness of wall and supporting system, construction activities and time and workmanship etc. However, such research in relation to Jakarta has been limited. Little reliable and well-documented data on the properties of soil

Responsible Editor: Zeynal Abiddin Erguler

✉ Bin-Chen Benson Hsiung
bensonhsiung@email.nchu.edu.tw

Fuchen Teng
fteng@mail.ntust.edu.tw

Muhammad Dwiyanto Agung Prakasa
dwiyantoagung17@gmail.com

Kuo-Hsin Yang
khyang@ntu.edu.tw

Anthony
anthony9_4@yahoo.com

Richard Litanes
r08521127@ntu.edu.tw

[1] Department of Civil and Construction Engineering, National Taiwan University of Science and Technology, Taipei 106, Taiwan

[2] Department of Civil Engineering, National Chung-Hsing University, Taichung 40227, Taiwan

[3] Department of Civil Engineering, State Polytechnic of Ujung Pandang, Makassar 90245, Indonesia

[4] Department of Civil Engineering, National Taiwan University, Taipei 106, Taiwan

[5] Department of Civil and Construction Engineering, National Taiwan University, Taipei 106, Taiwan

in the city have been obtained. Moreover, most deep excavation reports have been written and published in the local language. Exploring the characteristics of deep excavation in the Jakarta area is thus difficult for numerous reasons.

It herein presents finite element (FE) analyses executed on two prominent cases of large-scale deep excavation in Central Jakarta. These cases, namely Cases A and B, were for sites separated by approximately 660 m. The subsurface soil had a thick clay deposit with an occasional sand lens. According to the field measurements made for both cases, substantial wall deformation occurred during the final stage of excavation, presumably due to clay's time-dependent behaviour, for example, creep and consolidation (i.e., dissipation of the excess pore water pressure). The reasons behind and mechanisms underlying the substantial wall deformation were explored in detail in this study.

In this paper, detailed background information on Cases A and B is first introduced, including monitoring data, the construction sequence, the results of field and laboratory soil tests, and the subsurface soil conditions. Cases A and B were both commercial projects, and the utmost effort was made by the authors to collect and explore all available and reliable data. This study conducted three-dimensional (3D) FE analyses to model the two cases, and the ability of these models to predict 3D wall displacement caused by excavation was determined. The soft-soil (SS) model and soft-soil-creep (SSC) model, two advanced soil models (details of two models will be explained in the later section), were employed to model clay's time-dependent behaviour and the effect of soil creep. Numerical analysis results and field measurements were compared, and the influence of clay's time-dependent behaviour on wall behaviour was assessed. A set of soil parameters were established for the two aforementioned models, and the creep index of Central Jakarta clay was proposed. This study further investigated the factors influencing the maximum rate of wall deflection, which was defined as the largest wall deflection divided by the time taken to construct the floor or base slab. The relationship of this rate with the excavation depth for Case A was compared with that in the case of the Taipei National Enterprise Centre (Ou et al. 1998) because both of these excavation processes were performed mainly in very thick clay and the construction method was a top-down approach. The present findings can be a useful reference for relevant personnel hoping to excavate in Central Jakarta in that they can help such personnel predict wall deformation by taking the time-dependent behaviour of soil into account.

Project background

Case A

Compared with Case B, Case A was more complex because of an inclined road embankment on one side of the excavation, surrounded by several high-rise buildings. In Case A, the construction sequence involved a top-down approach and comprised four excavation stages, with support from a reinforced concrete slab comprising four layers of differing thickness. The excavated area had 190-m length and 21-m width. A diaphragm wall was used as a retaining structure, and it had 1.2-m thickness and 33.7-m depth.

The diaphragm wall was installed in the first stage of construction, and this was followed by excavation of soil to ground level (GL). Afterwards, a B1F slab, for which the thickness was gauged to be 0.8 m, was placed 3.90 m below GL. In the second stage of excavation, soil was removed to 11.00 m below GL, and a B2F slab with a 0.4-m thickness was installed at 10.20 m below GL. The third and fourth excavation phases were performed similarly. Finally, a 1-m-thick B4F slab was cast. Table 1 presents the complete construction sequence for Case A.

Case B

Case B was located 660-m north of Case A, and the top-down construction method was again used. The excavation was determined to have a total length of 429.5 m, a width varying from approximately 26 to 30 m, and a depth varying from approximately 18 to 20 m. A diaphragm wall, for

Table 1 Process of construction for Case A

Stage	Construction sequence	Time (days)
1	Installation of diaphragm wall	150
2	1st excavation stage to the depth GL. -4.90 m	5
3	B1F slab installation at GL. -3.90 m (slab thickness, $t = 0.8$ m)	20
4	2nd excavation stage to the depth GL. -11.00 m	14
5	B2F slab installation at GL. -10.20 m (slab thickness, $t = 0.4$ m)	29
6	3rd excavation stage to the depth GL. -16.90 m	13
7	B3F slab installation at GL. -16.10 m (slab thickness, $t = 0.4$ m)	41
8	4th excavation stage to the depth GL. -24.85 m	20
9	B4F slab installation at GL. -24.05 m (slab thickness, $t = 1$ m)	56

which the thickness and depth were gauged to be 1.0 and 24.1 m, respectively, was employed as a retaining wall. Figure 1a depicts the plan view of excavation Case B. In the present numerical analyses, Section E-E was selected for study. More details on Case B were presented by Hsiung et al. (2018).

Figure 1b presents the excavation cross section and ground profile for Section E-E in Case B. The width and excavation depth of this section were respectively 22.6 and 18.93 m. Excavation was performed in five stages until the maximum depth of excavation was reached. The retaining wall was supported by three levels of reinforced concrete slabs with different thicknesses for the various levels.

The first task entailed constructing the diaphragm wall as well as the king post and then excavating the soil to 1.50 m below GL. Subsequently, a deck slab with 0.4-m thickness was cast at GL. In the second stage of excavation, soil was removed to 5.08 m below GL, and a 0.8-m-thick top slab was installed at 4.18 m below GL. The next steps were soil excavation to 11.18 m below GL and placement of a middle slab at

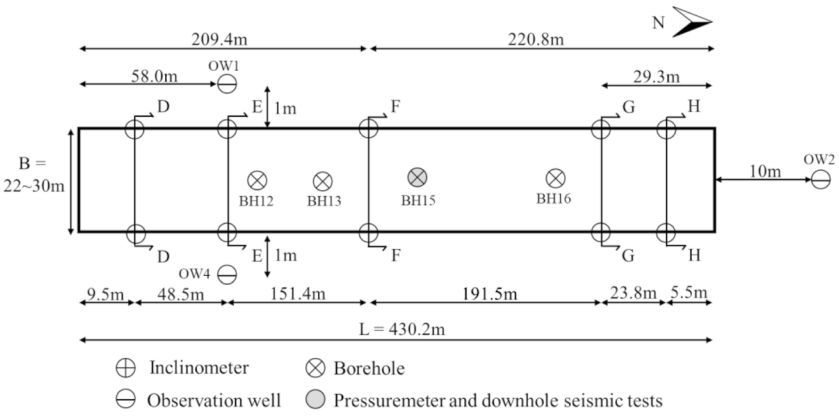

(a) Site layout, activities, and location of analytical section in Case B

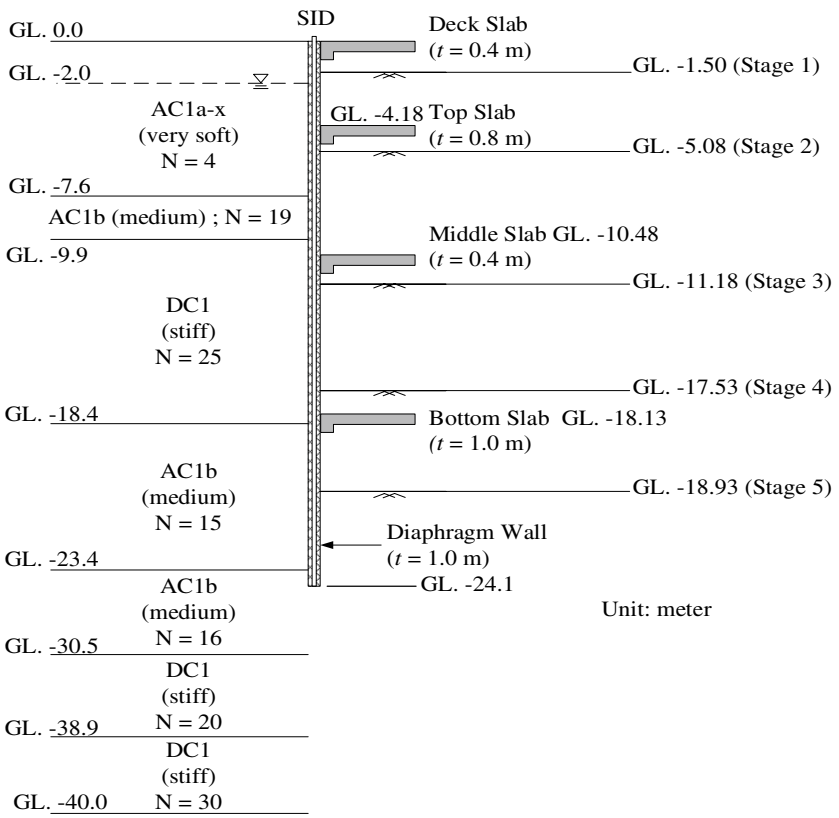

(b) Ground profile and cross section E-E of excavation in Case B

Fig. 1 Excavation Profile of Case B. (**a**) Site layout, activities, and location of analytical section in Case B. (**b**) Ground profile and cross section E-E of excavation in Case B (Hsiung et al. 2018)

10.48 m below GL. Last was placement of a 1.0-m-thick bottom slab at 18.13 m below GL. Table 2 provides comprehensive details on the sequence of construction for this section.

Geotechnical characteristics of soil

Geological formation

In Jakarta, quaternary and tertiary deposits are the main content of soils (Firmansyah and Sukamta 2000). Formed from volcanic ash, the quaternary deposit comprises three layers: a lower lahar comprising cemented silty sand and with a thickness of approximately 5 m; a layer in which silty clay, silty sand, and sandy silt alternate; and an upper lahar with a thickness of 3–5 m. The tertiary deposits are present from GL to a depth of more than 100 m and comprise thick greenish clay and silt, occasionally with a sand lens. Younger and Cook (Younger and Cook 1994) mentioned that the bonding of particles due to weathering can produce an "overconsolidation" effect. However, the size of this effect must be carefully assessed in terms of in situ and remolded void ratios and strength.

Site investigation and subsurface soil conditions

Nine boreholes were drilled in Case A. Figure 2a displays the standard penetration test (SPT)-N values for the boreholes closest to the observed section in Case A. The SPT-N values of the layers located at depths of 0–4 m was approximately 4 to 12. This layer could thus be classified as a medium-to-stiff clay layer (Younger and Cook 1994). The soil layer at 4–55 m below GL had high SPT-N values of 10 to 50 and was thus categorized as a stiff-to-hard clay layer.

Table 2 Construction phases and sequences of the excavation for Case B

Phases	Construction sequences	Elapsed days
1	Diaphragm wall installation	101
2	1st excavations to the depth of GL. -1.5 m	18
3	Deck slab installation at ground level (slab thickness, $t = 0.4$ m)	20
4	2nd excavation to the depth of GL. -5.08 m	30
5	Top slab construction at GL. -4.18 m (slab thickness, $t = 0.8$ m)	14
6	3rd excavation to the depth of GL. -11.18 m	22
7	Middle slab construction at GL. -10.48 m (slab thickness, $t = 0.4$ m)	20
8	4th excavation to the depth of GL. -17.53 m	28
9	5th excavation to the depth of GL. -18.93 m	28
10	Bottom slab construction at GL. -18.13 m (slab thickness, $t = 1.0$ m)	21

Figure 2a depicts the index properties of soils in Case A. Most of the soil was discovered to have water content near the plastic limit. Specifically, the ranges of the water content and plastic limit were 25.8%–85.4% and 25.6%–44.8%, respectively. The void ratio was between 0.75 and 2.4 and was found to be higher at smaller depths: approximately 2.0 and 1.0 at 15 and 22.5 m below GL, respectively. Moreover, the ratio was constant at 1.0 until 30 m below GL. At a greater depth, the soil was stiffer.

In Case B, field tests were conducted by drilling 10 boreholes. The SPT-N values from the three boreholes are summarized in Fig. 2b. These values were lower than 10 for a layer located at 0 to approximately 7 m below GL. On the basis of the criteria specified by Terzaghi et al. (Terzaghi et al. 1996), this layer was classified as soft clay. The SPT-N value increased (corresponding to stiffening) to 50 at a depth of 13 m and was then constant at an average of 30 for the layer located at 20–40 m.

The index properties of the soil in Case B are displayed in Fig. 2b. The soil could be clearly classified as predominantly clay. Furthermore, its natural water content was discovered to be 34.6%–89.3%, which approximated or exceeded the plastic limit. Both the plastic limit and liquid limit decreased gradually with increasing depth. This indicated that at greater depth, the shear strength may also be greater. The field test results revealed that the main soil at these sites was noted as being clay and separable into two layers, namely an upper layer (soft clay) and lower layer (stiff clay), on the basis of the SPT-N values in both cases.

Instruments installed at the site and behavior induced by the excavation

Instruments were installed at the sites of Cases A and B to explore the behavior induced by deep excavation; the instruments and performance for Case B were fully described by Hsiung et al. (Hsiung et al. 2018). Thus, only instruments that obtained reliable data for Case A are reported and analyzed in this section of the paper. The plan view and layout of the instruments employed in Case A are displayed in Fig. 3. The installed instruments included inclinometers in the wall, ground settlement nails, and observational wells.

For Case A, all surface and structural settlement remained the same for the whole excavation, around 5 mm, regardless of how far the location was from the excavation, which is unlikely; the appearance of settlement nails on the surface is shown in Fig. 4. Heavy traffic on the main road (Fig. 4) and the quality of settlement nails were strongly suspected to be reasons for the low quality of the surface settlement measurements. Thus, the measured surface settlement is not discussed herein.

The available lateral wall displacement data measured during various stages are presented in Fig. 5 (Fig. 3 shows the locations of inclinometers). Most of the inclinometer

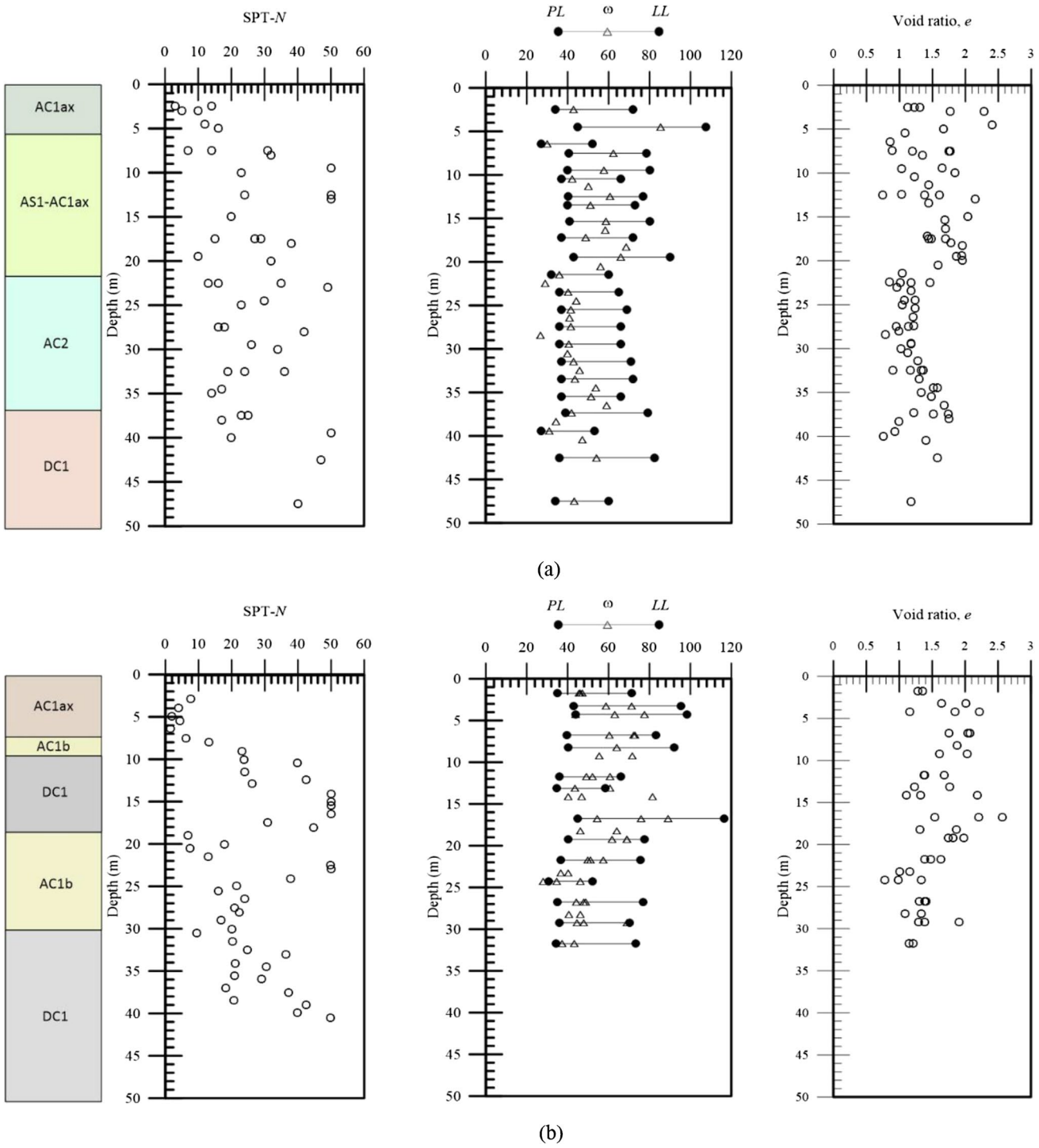

Fig. 2 Profiles of borehole log information for Cases. (**a**) Case A. (**b**) Case B (Hsiung et al. 2018)

measurements had similar trends; they began in the cantilever mode, which determined a maximum displacement in the range of 2 to 4 mm at the top of the wall, and then changed to the prop mode, which determined a maximum displacement in the range of 10 to 24 mm upon completion of the B4F slab. From the observations, the plane strain ratio (PSR)—derived as the quotient between the maximum wall displacement 7 m from the corner and the maximum wall displacement under a planar strain—was derived to be approximately 0.4. By considering the distance to the corner and excavation geometry, this study could interpret the PSR on the basis of the outcomes of Hsiung et al. (Hsiung et al.

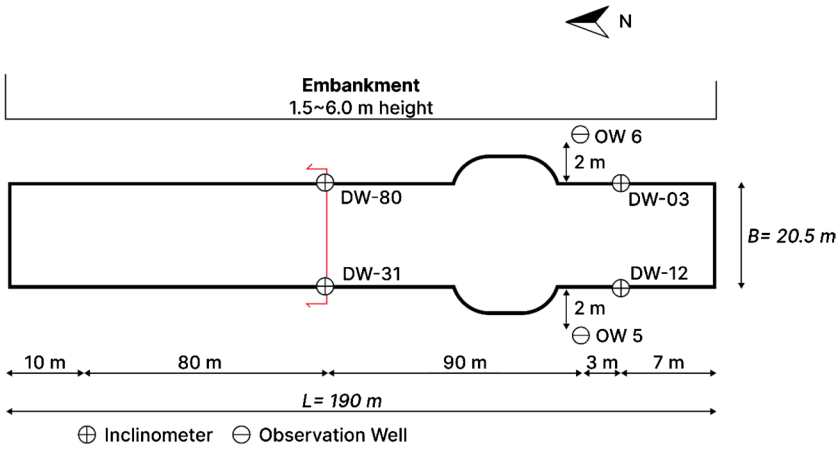

Fig. 3 Site layout and location of analytical section in Case A (**a**) Settlement nail on the ground (**b**) Traffic on the main road at the site

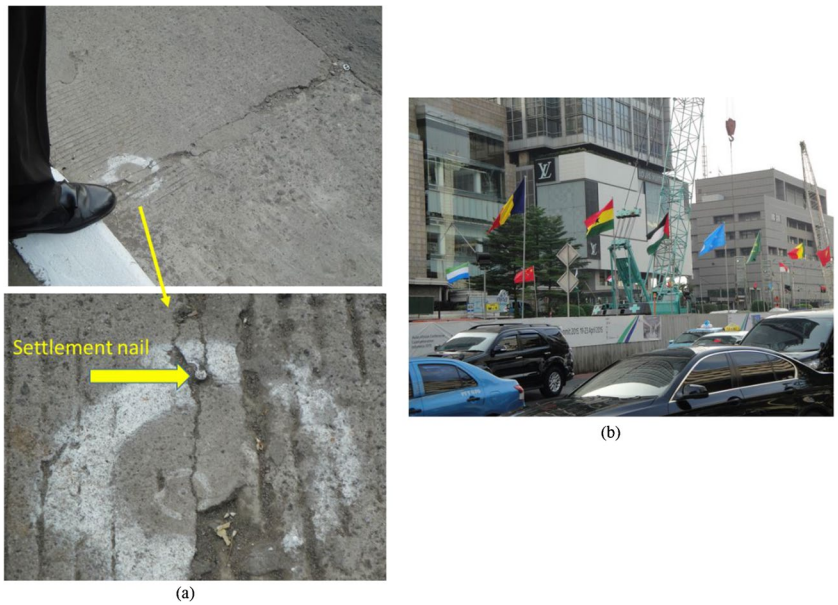

Fig. 4 Observations of instruments and traffic from project's site. (**a**) Settlement nail installed on the ground surface. (**b**) Traffic on the main road at the site

2018), and the derived values were found to not differ considerably from the ratio obtained from the observations for Case A. The influence of the corner effect was anticipated to lead to a reduction of the lateral wall displacement measured from inclinometers DW03 and DW12.

Figure 6 presents observations of the lateral wall displacement immediately and 1 month after B4F slab completion; it reveals that the wall displacement increased dramatically over that 1 month. The maximum wall displacement reached 26.1–46.3 mm after that month. Details and the reason are explored in a later section.

The water levels in two observation wells outside the excavation are displayed in Fig. 7, indicating similar trends. Specifically, the water level rose gradually from December 2014 to February 2015 and then dropped. November to February is generally the rainy season in Jakarta, and the press reported that flooding caused by rainfall caused some deaths in January and February 2015; thus, heavy rainfall during that period was the reason for the rising water level.

The water level continued to decrease after the main excavation was begun. Although the observation wells were located outside the excavation (~ 2 m away) and the excavation mainly removed impermeable clay with no pumping activities conducted, an embedded wall that was not sufficiently deep might not have fully prevented the impact of excavation-induced stress on the soil behind the wall, and this could have led to the generation of negative excess pore pressure. The water level thus dropped. Additionally, the water level started to recover from October 2015 (Fig. 7), and dissipation of the negative excess pore pressure took approximately 4 months.

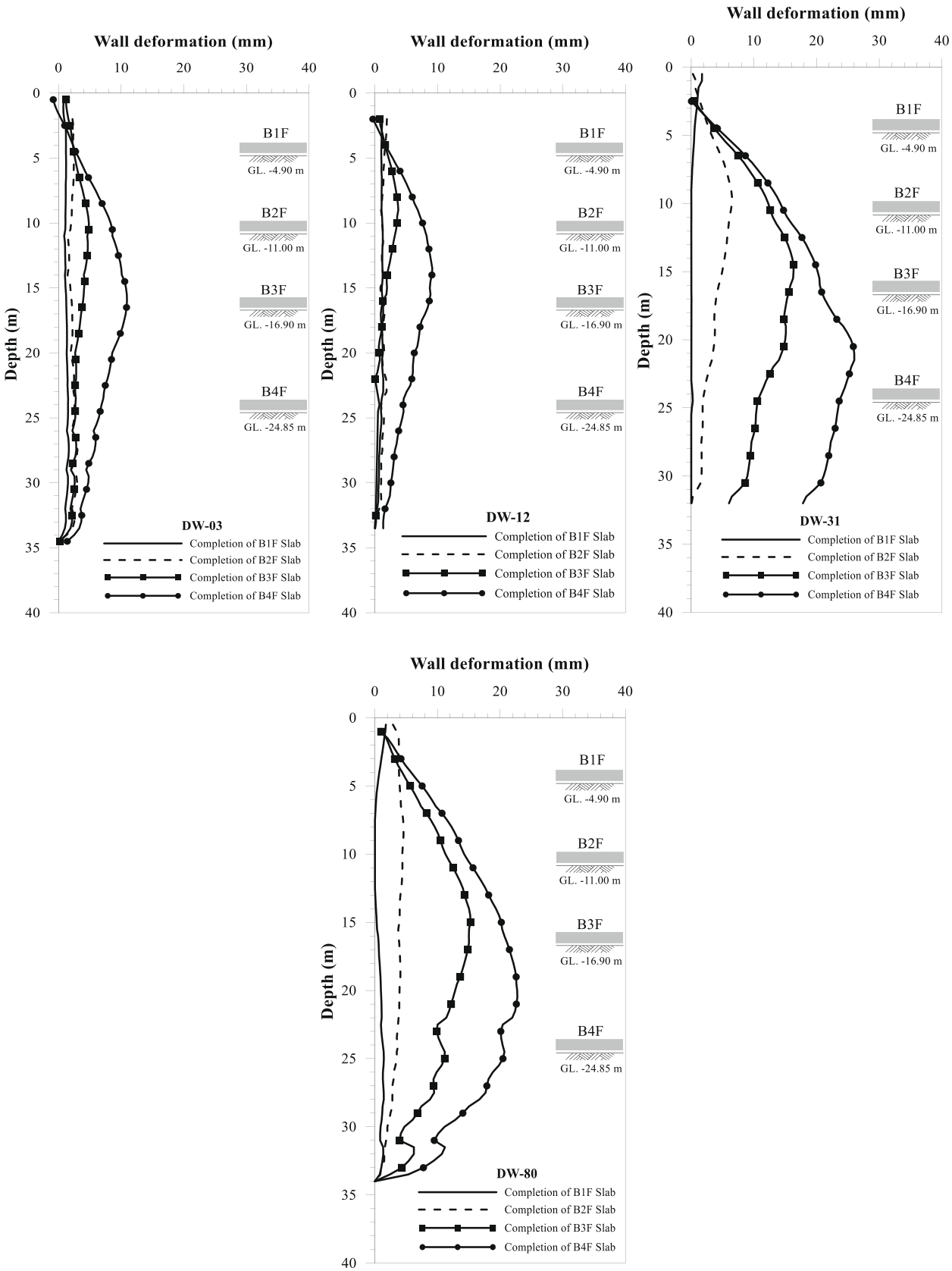

Fig. 5 Lateral wall displacement measured using various inclinometers in Case A

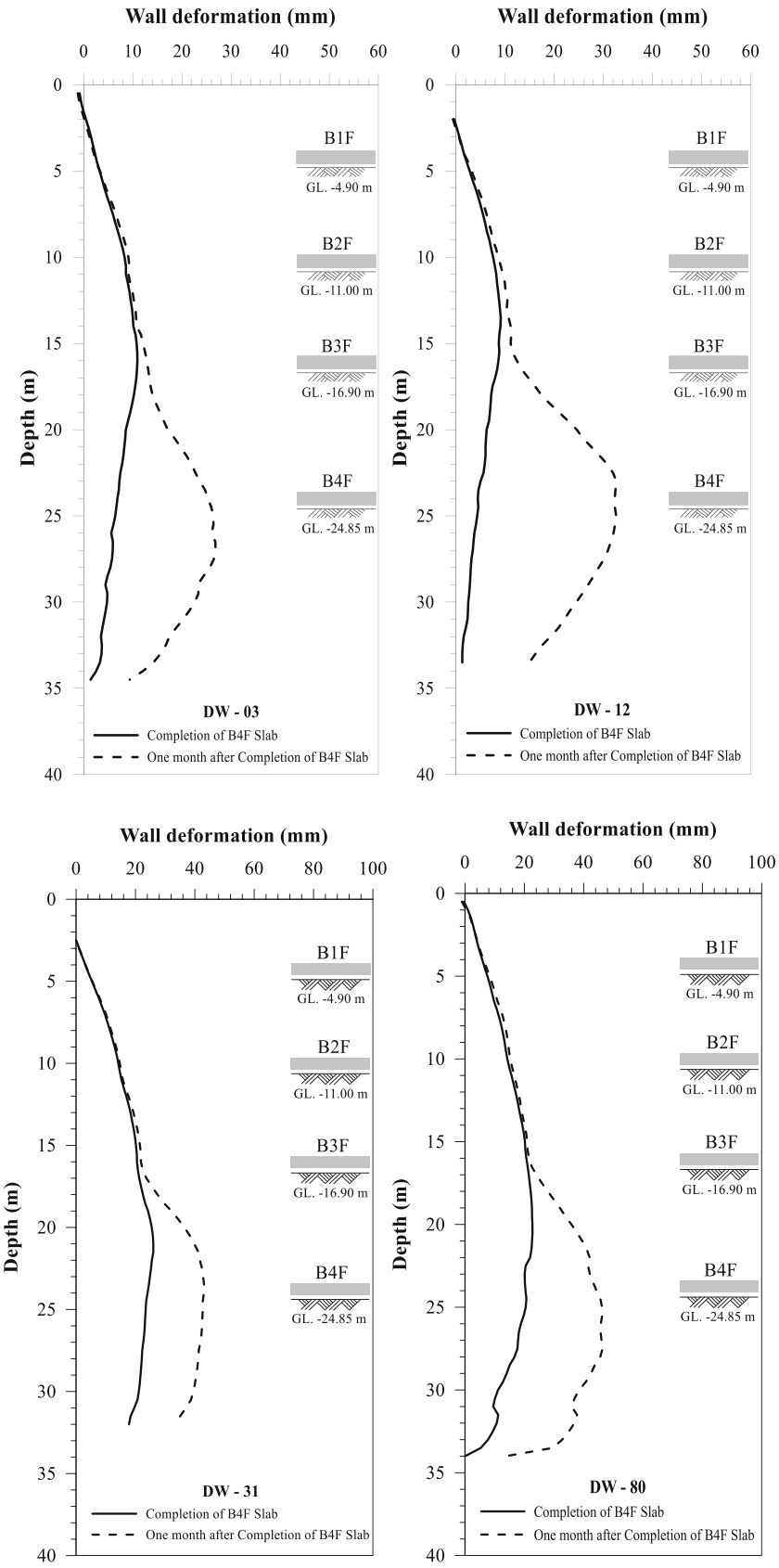

Fig. 6 Lateral wall displacement measured upon completion of B4F slab and 1 month subsequently

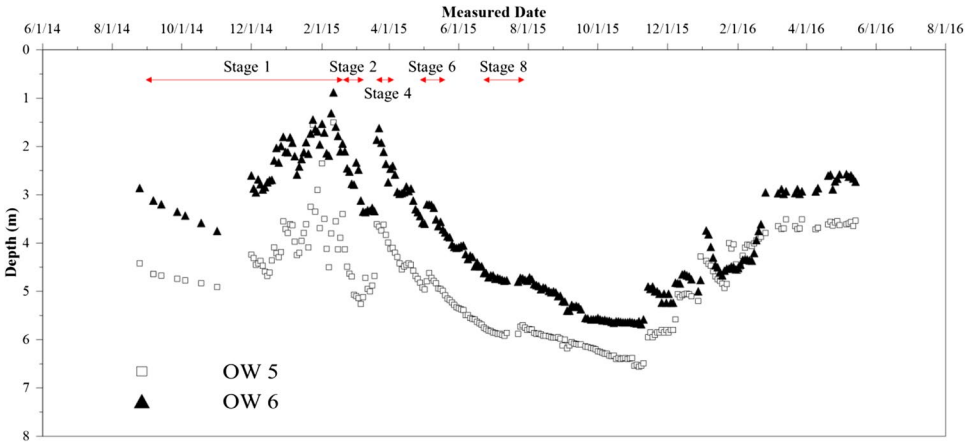

Fig. 7 Groundwater level outside the excavation during the various construction stages (indicated by arrows)

Numerical analyses

This study executed FE analyses by employing PLAXIS. To examine the full-scale excavations, the 3D approach was performed using PLAXIS 3D. Two constitutive models were employed in this analysis, namely the soft-soil and soft-soil-creep models. The numerical models for both cases are presented in Fig. 8. The models for Cases A and B had 25,370 and 14,007 elements, respectively. The model for Case A was a nonsymmetric full model with a road embankment on one side; the modeled volume was 340 m long, 320 m wide, and 65 m deep. The vertical boundary conditions were set to preclude horizontal movements, and the base was fixed in

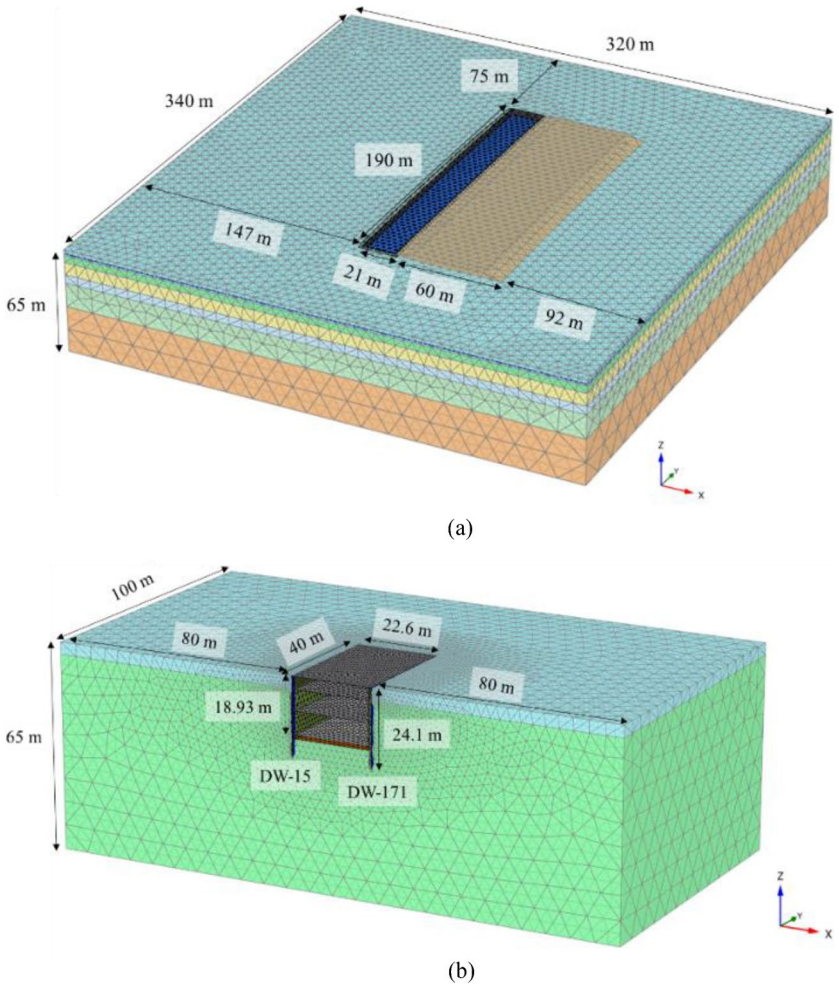

Fig. 8 FE model for Cases. (**a**) Case A. (**b**) Case B

Table 3 Soil parameters for the soft soil and soft coil creep models

Parameters	Symbol	Unit	Upper clay (0 – 3.80 m)	Lower clay (3.80 – 65.00 m)
Saturated unit weight	γ_{sat}	kN/m^3	15.46	16.67
Unsaturated unit weight	γ_{unsat}	kN/m^3	15.46	16.67
Initial void ratio	e_{init}		1.51	1.62
Effective cohesion	c'	kN/m^2	6	3.5
Friction angle	φ'	^{o}	38	39
Dilatancy angle	ψ	^{o}	-	6.5
Modified compression index (adjusted λ*)	λ*		0.1039 (0.05197)	0.04647 (0.01859)
Modified swelling index (adjusted κ*)	κ*		0.02772 (0.01039)	0.003319 (0.002655)
Modified creep index	μ*		0.003464	0.00195
Compression index	C_c		0.6	0.28
Swelling index	C_s		0.08	0.01
Creep index	C_α		0.02	0.01175
Over-consolidation ratio	OCR		2–4	1–2.5
Permeability	k	m/day	0.063	5×10^{-5}

all directions. For Case B, a symmetric half-model was constructed and had a 100-m length, 182.6-m width, and 65-m depth. There are several options to conduct calculation analysis in PLAXIS, which are plastic, consolidation, and safety calculation. In this study, consolidation analysis is employed in all stage of construction. Consolidation calculation is used to capture the behavior of the soil which are mostly low permeability clay.

Soil constitutive model and input properties

So called the soft-soil model is based on the modified Cam-clay model and adopts the Mohr–Coulomb failure criterion. The main difference between two models listed above is additional reference pressure has to be considered once soil parameters used for SS model are adopted but not for a conventional modified Cam-clay model. The soft-soil-creep model corresponds essentially to an extension of the soft-soil model that enables it to recognize soil's time-dependent behavior (secondary compression). The triaxial consolidated undrained test was employed to obtain strength parameters (friction angle and effective cohesion), which were calibrated to maximize the input parameters' performance. Oedometer testing revealed that the compressibility index (C_c) was in the range of 0.28–0.81. Once parameter calibration was complete, the selected C_c was 0.6 for the upper layer and 0.28 for the lower layer. The swelling index (C_s) was determined using the equation from Edil et al. (Edil et al. 2009). Accordingly, C_s was set to 0.08 for the upper layer and 0.01 for the lower layer. Bakr (Bakr 2015) proposed values of 0.005–0.03 for the secondary compression index (C_α) for Jakarta clay. In the present analysis, the C_α values for the upper layer and lower layer were 0.02 and 0.012, respectively. The stiffness parameters (λ^*, κ^*, and μ^*) for the soil models were obtained using the C_c, C_s, and C_α values through empirical correlation (Bakr 2015) as follows:

Table 4 Material properties of the diaphragm wall for Case A

Parameter	Symbol	Value	Unit
Compressive strength of concrete	f'_c	21	MPa
Equivalent thickness	d	1.2	m
Young's modulus	E	21.7×10^6	kPa
Normal stiffness	$0.8EA$	20,640,000	MPa
Bending stiffness	$0.8EI$	2,470,000	
Unit weight	ω	9.522	kN/m^3
Poisson's ratio	υ	0.15	-

Table 5 Material properties of the diaphragm wall for Case B

Parameter	Symbol	Value	Unit
Compressive strength of concrete	f'_c	21	MPa
Thickness	d	1	m
Young's modulus	E	21,700	MPa
Young's modulus 70%	$0.7E$	15,200	MPa
Unit weight	γ	6	kN/m^3
Poisson's ratio	υ	0.15	-

Table 6 Input parameters for the concrete slab for Case A

Slabs	d (m)	υ	80%E (MPa)
B1F	0.8	0.15	13.4×10^6
B2F	0.4	0.15	6.72×10^6
B3F	0.4	0.15	6.72×10^6
B4F	1	0.15	16.8×10^6

Table 7 Input parameters for the concrete slab for Case B

Slabs	*d* (m)	υ	80%E (MPa)
Deck slab	0.4	0.15	17,400
Top slab	0.8	0.15	17,400
Middle slab	0.4	0.15	17,400
Bottom slab	1	0.15	17,400

$$\lambda^* = \frac{C_c}{2.3(1+e)} \tag{1}$$

$$\kappa^* = \frac{1.5C_s}{2.3(1+e)} \tag{2}$$

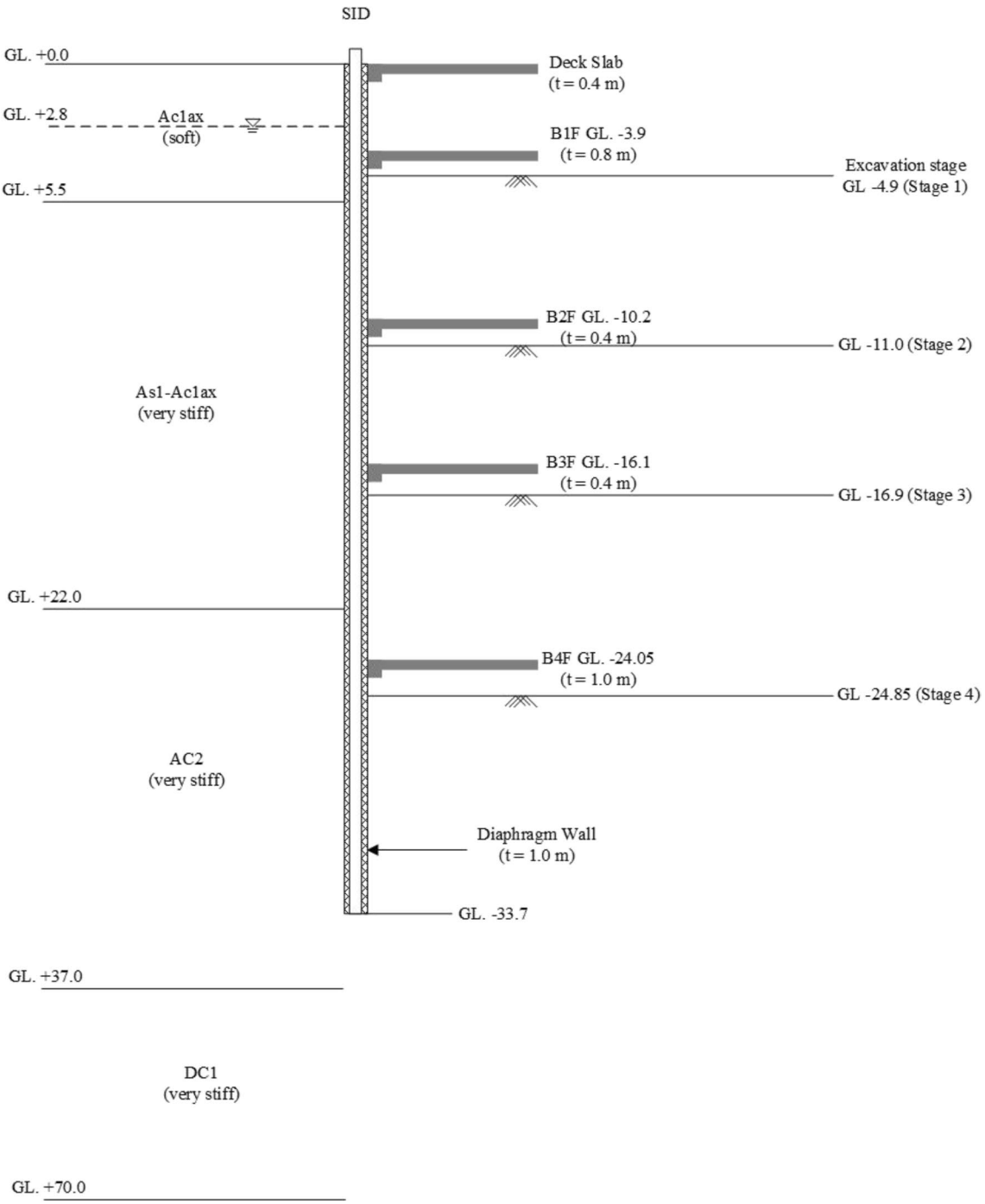

Fig. 9 Ground profile and cross section of excavation in Case A

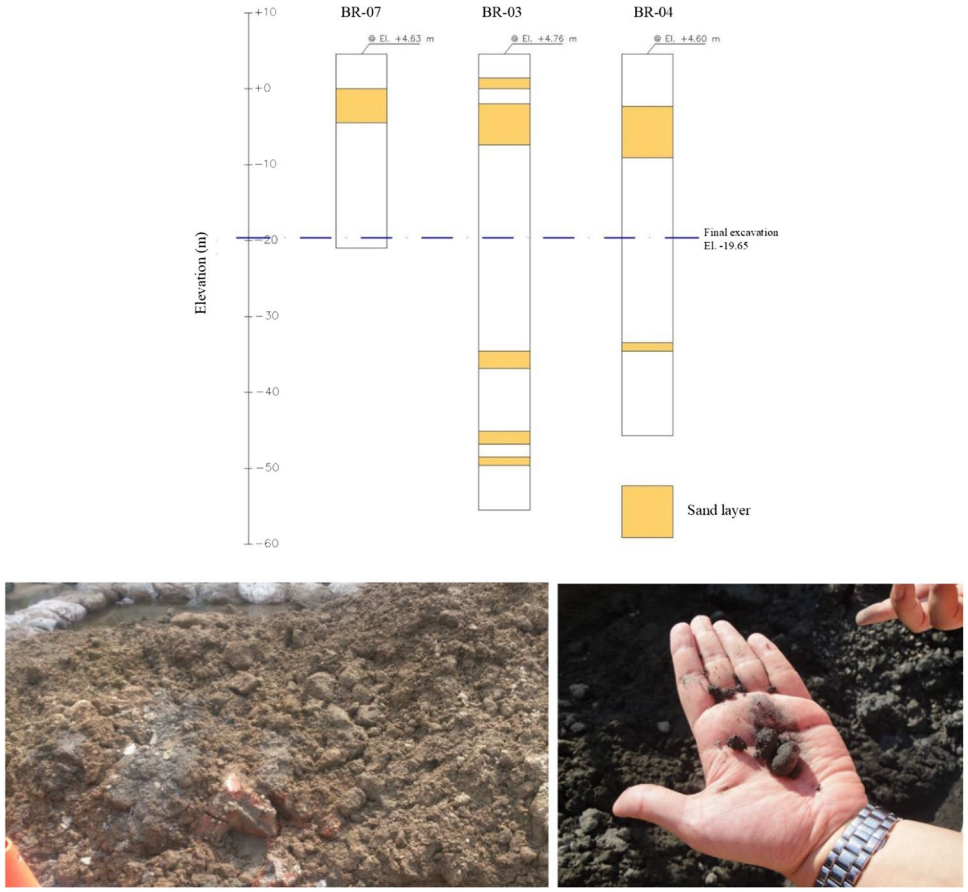

Fig. 10 Soil logs and soils for Case A

$$\mu^* = \frac{C_\alpha}{2.3(1+e)} \tag{3}$$

where e denotes the void ratio and λ^*, κ^*, and μ^* denote the modified compression, swelling, and creep indices, respectively.

Additionally, this study set the Poisson's ratio (υ) to 0.2 because the soil was categorized as stiff clay. The entire list of soil parameters used as input for the two models is provided in Table 3.

In the present analysis, the structural elements (diaphragm wall and concrete slab) were simulated using plate elements. The following equation from the American Concrete Institute was applied to calculate the Young's modulus (E) of concrete:

$$E = 4700\sqrt{f_c'}(\text{MPa}) \tag{4}$$

where f_c' is the concrete's compressive strength after 28 days of curing (unit, MPa). The degree of unit weight and volume overlap between soils and another material such as concrete and steel was compensated by subtracting the soil unit weight from the material's real unit weight. The diaphragm wall thickness for both cases was 1.0 m, with the depth being 33.7 and 24.2 m for Cases A and B, respectively. Ou (Ou 2006) stated that when cracks in the retaining wall are considered, the diaphragm wall's stiffness (EI) is usually 20% to 40% lower due to the bending moment. Accordingly, the stiffness of the diaphragm wall for Cases A and B was 20% and 30% lower, respectively. This wall's material properties in both cases are detailed in Tables 4 and 5.

When construction is performed in the top-down manner, concrete slabs can have a 20% lower axial stiffness; this corresponds to the quality of concrete compressive strength in the field (which may differ from the designed strength) as well as cracking issues (Ou 2006). The input parameters for the concrete slab in both cases are presented in Tables 6 and 7. Soil's interaction with structural elements, specifically the diaphragm wall, was simulated in the models by employing interface elements (R_{inter}). Waterman (Brinkgreve et al. 2017) and Hsiung et al. (Hsiung et al. 2018) have suggested that R_{inter} values for clay–concrete interaction is 0.5–1.0. Therefore, the present numerical analyses were performed using the average value of R_{inter} (0.7).

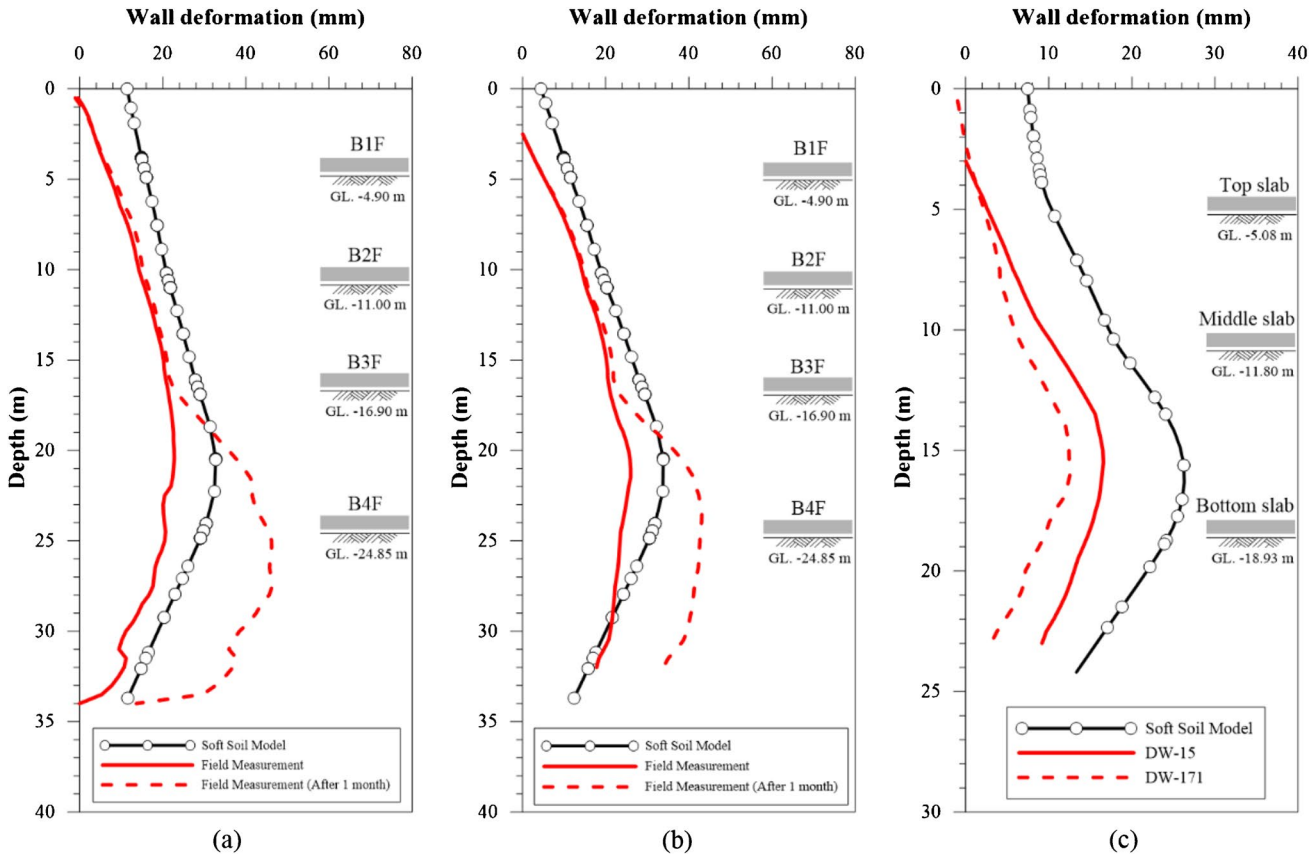

Fig. 11 Wall deformation in the final stage. (**a**) Case A (embankment side). (**b**) Case A (no-embankment side). (**c**) Case B

Analysis results and back analysis of parameters

The section in the middle of Case A (Fig. 3; Section DW-30 to DW-81) and Section E-E in Case B as shown in Fig. 4 were selected to further compare the simulation and field monitoring results. Figure 9 illustrates the excavation cross section and ground profile at the aforementioned section in Case A. The soil logs as depicted in Fig. 10 revealed several layers of permeable sand at the project site, although these layers were not fully shown in the ground profile used for analyses (Fig. 9).

The simulation results for the lateral wall displacement in the final stage are illustrated in Fig. 11. As displayed in the figure, the maximum wall deformation levels determined in the final stage at the no-embankment and embankment sides in Case A were respectively 33.8 and 32.7 mm. The results obtained in the numerical simulation tended to be slightly larger than the field measurements made after the completion of the slab. In Case B, the lateral wall deflection in the final stage was 26.3 mm, larger than the measurements made by the inclinometer. The soft-soil model implemented using the parameters listed in Table 3 did not reveal results that favorably matched the observations for either case. Thus, the parameters were calibrated through back analyses.

The parameters for the soil model, such as λ^* and κ^*, were initially determined through calibration with triaxial tests and oedometers (Fig. 12). The overconsolidation ratio values were determined to be consistent with those reported by Kooi and Erkens (Kooi and Erkens 2020) for the clay in Jakarta. However, the geotechnical characteristics of the two excavations could be examined most clearly through back analysis. In this analysis, the simulation results were matched with the field measurements for Case A, which served as the reference case. The analysis was performed by adjusting the stiffness parameters (λ^* and κ^*) until the generated wall deformation fit the inclinometer reading. Subsequently, the adjusted parameters, λ^* and κ^*, were also applied to Case B. The adjusted λ^* and κ^* for the soft-soil model are shown in Table 3.

The wall deflection obtained through the back analyses executed for both cases in the final stage is shown in Fig. 13. The simulation results were a relatively good fit to the field measurements made on both sides after the completion of the slab for Case A. For Case B, the lateral wall displacement was slightly larger than the field measurement. The maximum wall deformation in the simulation was 20.6 mm, whereas that in the field measurements was 16.6 mm. Generally, the soft-soil model

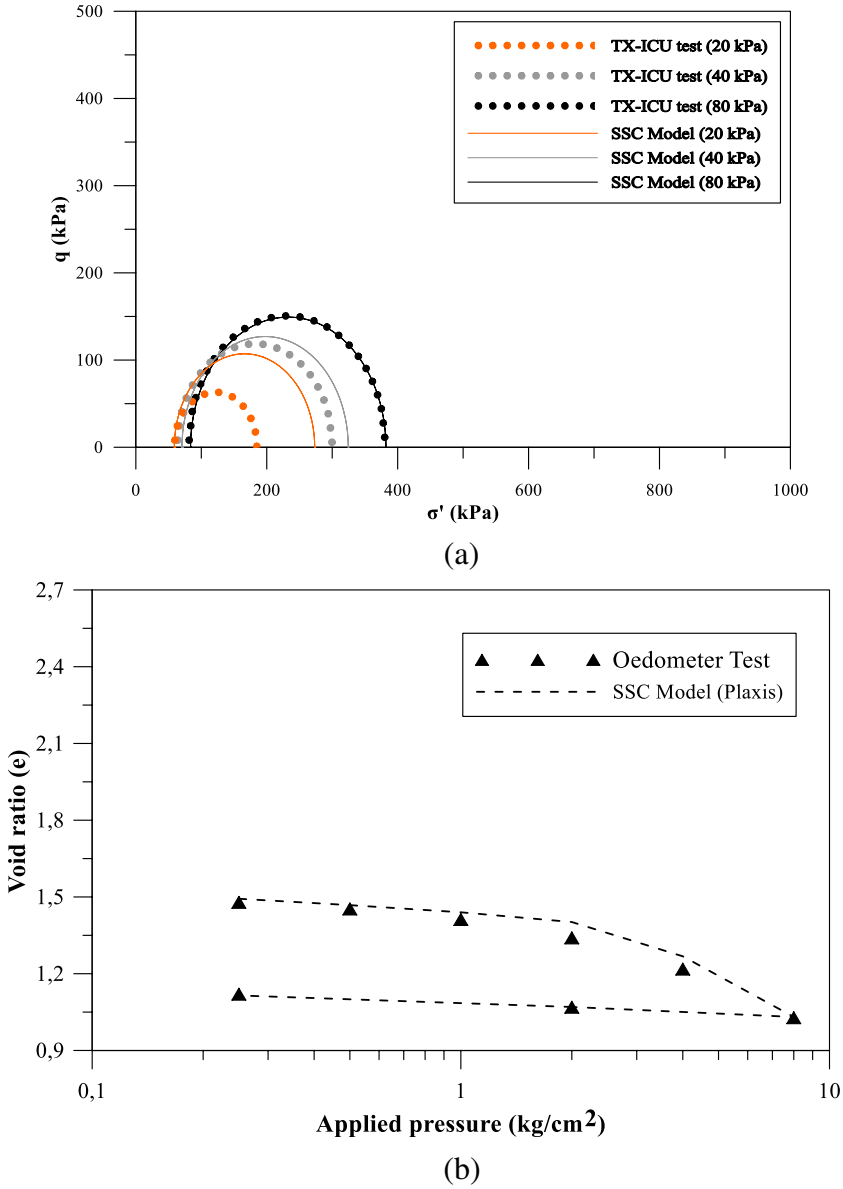

Fig. 12 Calibration of λ^* and κ^* parameters. (**a**) Calibration of λ^* and κ^* with a triaxial test. (**b**) Calibration of λ* and κ* with oedometer test

with the calibrated soil parameters could favorably predict ground movements for both cases. The calibrated parameters were employed in subsequent analyses with the soft-soil-creep model to investigate the effects of creep and consolidation.

Effect of soil creep

The definition of creep is an increase in the shear strain over time under constant external stress (Terzaghi et al. 1996). Long-term time-dependent ground deformation was observed for an excavation in Cleveland, the United States (Wu et al. 1978), and the creep behavior of the soft clay was suggested to be the cause. According to observations made during excavations, walls around the excavated volume and the ground generally continue to deform as time passes after the completion of the excavations, and these deformations can lead to failure (Lin 1992). Lin and Wang (Lin and Wang 1995) reported that soil creep had a significant effect on excavations in Taipei. Hence, the influence of clay's time-dependent behavior on an excavation must be considered. Studies on the creep of Boom clay—stiff clay found near the city of Mol in Belgium—were recently conducted by Yu et al. (Yu et al. 2015), who described the impacts of several factors, such as the confining pressure and deviator stress. The results of laboratory tests and in situ measurements indicated that Boom clay (i.e., stiff clay) is also highly likely to creep.

Excavations in Indonesia are generally completed using a top-down method. In this procedure, forms are built, and a

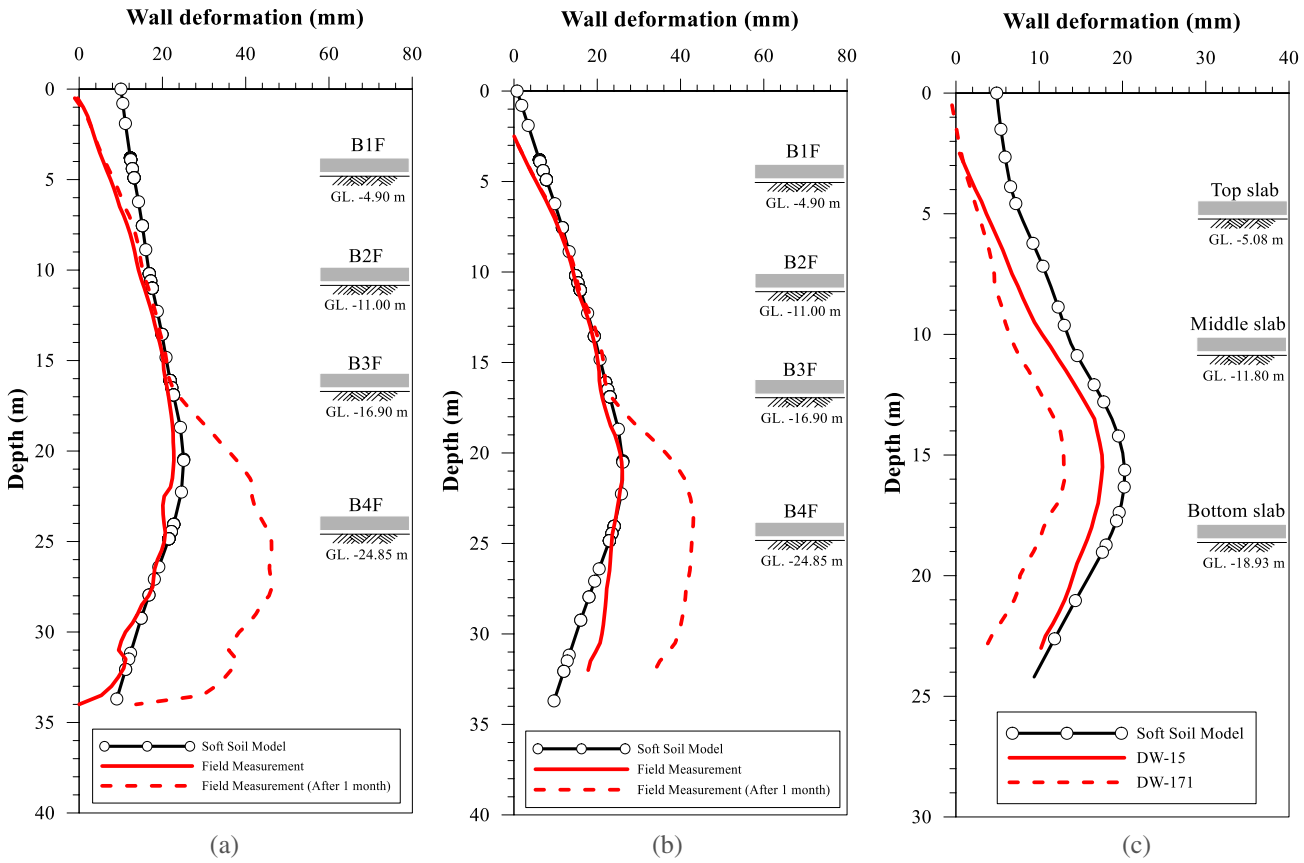

Fig. 13 Wall deformation in final stage after back analysis. (**a**) Case A (embankment side). (**b**) Case A (no-embankment side). (**c**) Case B

concrete slab is poured before the next step is begun, and this takes considerable time. The retaining structure can deform considerably during waiting periods, which are periods in which no excavation activities are being performed. The wall displacement that occurs during the waiting period has been found to add up to 30% of the total deflection, and soil creep was discovered to contribute considerably to this addition (Ou et al. 1998; Lin et al. 2002). A recent study performed

Table 8 Stages of construction in the numerical analyses

Phase	Stage of construction	Flow condition (Water level)		Time
		Excavation side	Retaining side	(days)
0	Initial phase	- 2.8 m depth	- 2.8 m depth	-
1	Construction of road embankment	- 2.8 m depth	- 2.8 m depth	7300
2	Installation of diaphragm wall	- 2.8 m depth	- 2.8 m depth	150
3	Excavate to -4.90 m depth	Dry to -4.9 m depth	- 2.8 m depth	5
4	Install B1F slab at -3.90 m depth	Dry to -4.9 m depth	- 2.8 m depth	20
5	Consolidation	Dry to -4.9 m depth	- 2.8 m depth	30
6	Excavate to -11.00 m depth	Dry to -11 m depth	- 2.8 m depth	14
7	Install B2F slab at -10.20 m depth	Dry to -11 m depth	- 2.8 m depth	29
8	Consolidation	Dry to -11 m depth	- 2.8 m depth	30
9	Excavate to -16.90 m depth	Dry to -16.9 m depth	- 2.8 m depth	13
10	Install B3F slab at -16.10 m depth	Dry to -16.9 m depth	- 2.8 m depth	41
11	Consolidation	Dry to -16.9 m depth	- 2.8 m depth	30
12	Excavate to GL. -24.85 m depth	Dry to -24.85 m depth	- 2.8 m depth	20
13	Install B4F slab at -24.05 m depth	Dry to -24.85 m depth	- 2.8 m depth	56
14	Consolidation	Dry to -24.85 m depth	- 2.8 m depth	30

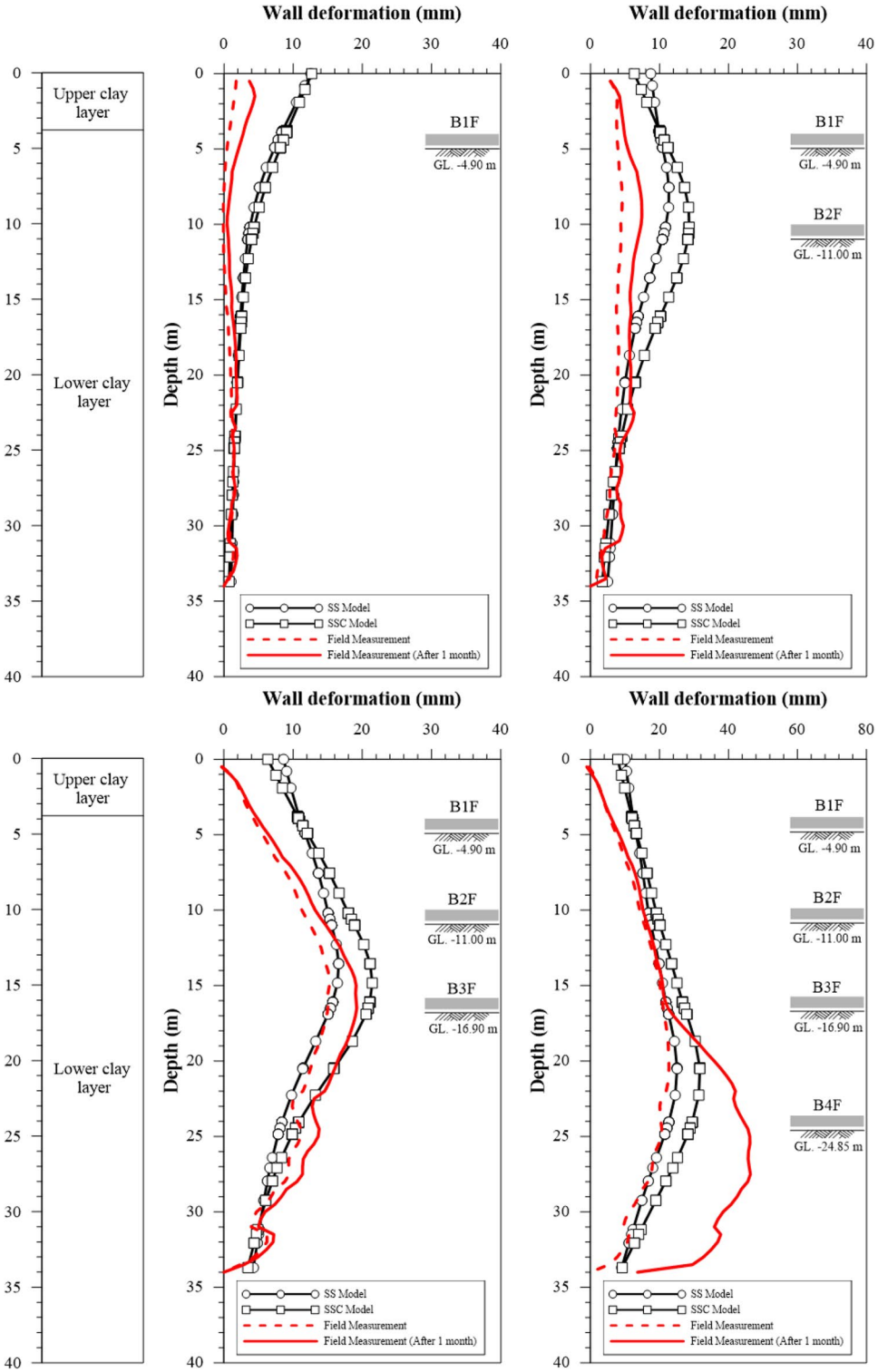

Fig. 14 Wall deformation results obtained using the SS and SSC models for the embankment side

by Harahap and Ou (Harahap and Ou 2020) confirmed the same finding obtained in studies of an excavation in Taipei.

In the present work, the time-dependent behavior of the Case A excavation was numerically analyzed using the soft-soil-creep model. In this simulation, construction consisted of 14 phases, as listed in Table 8. An additional phase involving 1 month of consolidation was added after the installation of slabs in order to probe the creep effect of soil when no excavation activities were taking place and during waiting periods. To address the time-dependent behavior of the soil, all phases were analyzed under the consideration of consolidation. The soil parameters from the back analyses (Table 3) were employed in the simulation.

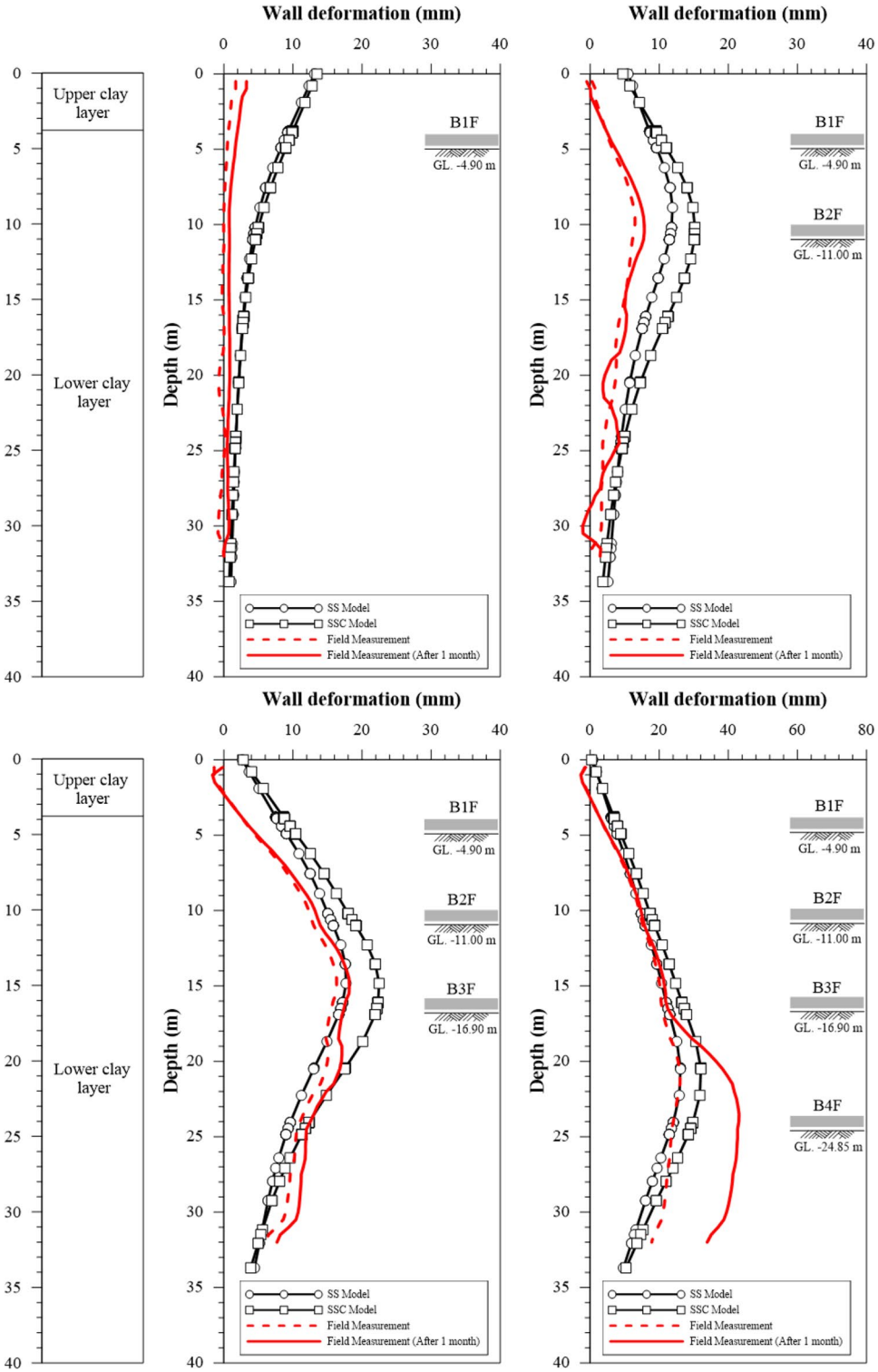

Fig. 15 Wall deformation results obtained using the SS and SSC models for the no-embankment side

The numerical results were compared with the field measurements for two time points: immediately after and 1 month after the completion of the slab. Figure 14 and 15 display the calculated lateral wall deflection at the embankment and no-embankment sides, respectively. For the first stage of excavation for both sides, the field measurements were smaller than the simulation results obtained using both soil models. This discrepancy was caused by the soil's behavior in a small strain range, which is a limitation of these models. The wall displacements obtained in the soft-soil and soft-soil-creep models were almost the same. The results revealed that creep did not occur in this phase, in favorable

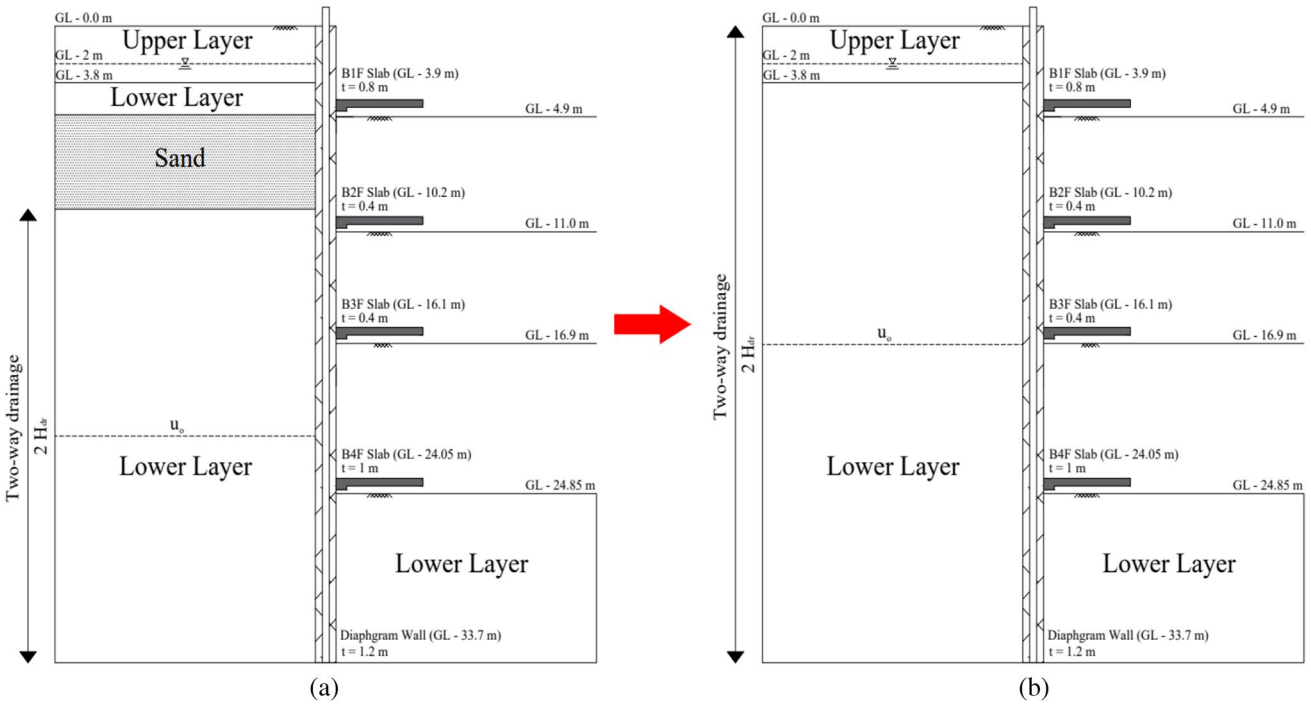

Fig. 16 Incorporation of the sand lens effect through Terzaghi's one dimensional consolidation. (**a**) Original. (**b**) Simplified ground conditions

agreement with the field measurements; there was no major difference between the inclinometer reading obtained when the slab had been completed and that obtained 1 month subsequently. The effect of soil creep began to appear in the next stage of construction; in the second stage of excavation, the soft soil creep-model-derived lateral wall deformation was larger than the soft soil-model-derived derived deformation. Thus, soil creep was responsible for the additional wall deformation at the final stage, constituting 23%–26% of the deformation. However, the simulation results were still smaller than the observations after the waiting period (i.e., 1 month after slab casting). This revealed that the creep effect was not the only factor causing the increase in wall deflection in the final stage. An additional factor may have been the rapid dissipation of excess pore water pressure due to the occasional presence of a sand lens in Case A. In this simulation, it is only observed the effect of soil creep on wall deformation and the effect of consolidation have not been considered. Thus, numerical simulations on soil consolidation were performed.

Effect of soil consolidation

Despite a time-dependent model being employed in the analyses, the wall deflection obtained using the soft soil creep model still did not match the field measurement (1 month after slab completion) for the final stage. The ground investigation results indicated local sand lenses at the site. The existence of sand lenses in the area influences the permeability of the soil and results in more rapid consolidation. The sand lenses were located 5 to 10 m below GL and below the diaphragm wall. In the interbedded clay layer located between the sand lenses, excess pore water pressure (u_o) can dissipate through two paths (two-way drainage). Therefore, Terzaghi's consolidation theory was used to increase the permeability of the clay layer because of the sand lenses' existence, and this was achieved by employing a parameter called the time factor (T_v). T_v is a nondimensional number that depends on the permeability (k), time (t), and maximum drainage path (H_{dr}). The idea is to incorporate the effect of sand lenses without actually modeling the lenses in the numerical simulation. Figure 16 shows the original ground condition and simplified ground condition. H_{dr} was determined for the initial and simplified ground conditions [$H_{dr(i)}$ and $H_{dr(eq)}$, respectively] accordingly. T_v and t were the same for both models. Hence, the initial permeability (k_i) was transformed into the equivalent permeability (k_{eq}) by using Eq. (5), which considers the influence of sand lenses. The equivalent permeability (k_{eq}) value of 0.0001 m/day was obtained and applied in the numerical model.

$$k_{eq} = k_i \frac{H^2_{dr\,(eq)}}{H^2_{dr(i)}} \tag{5}$$

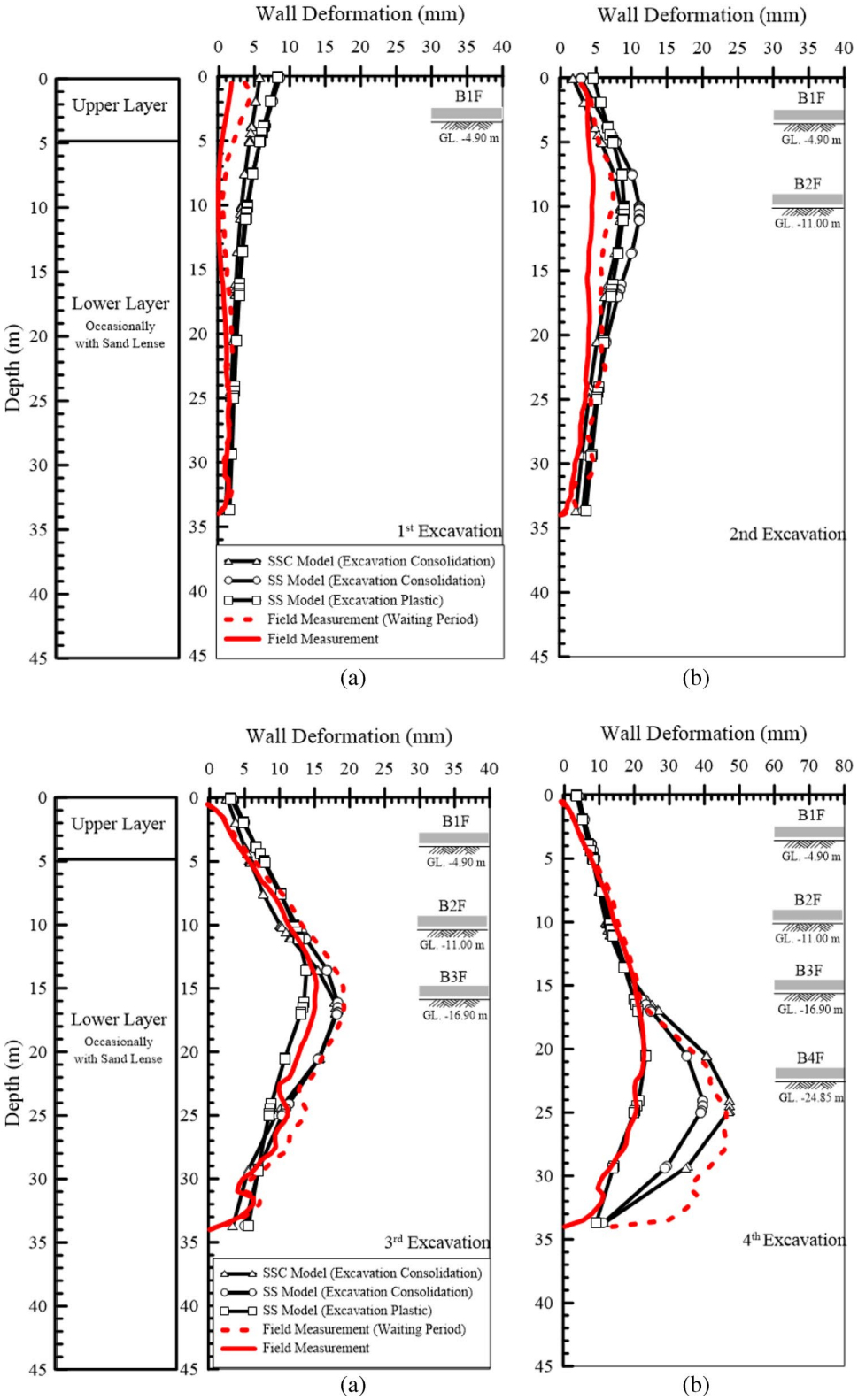

Fig. 17 Wall deformation results obtained using the SSC model (with sand lenses added) for the embankment side

Brinkgreve et al. (Brinkgreve et al. 2017) stated that the response of soil in consolidation analysis is determined by its permeability rather than the type of drainage. Accordingly, the lower layer was considered to have the undrained drainage type. The numerical results obtained for the embankment and no-embankment sides are displayed in Fig. 17 and 18, respectively. The simulation results were consistent with the field measurements made 1 month

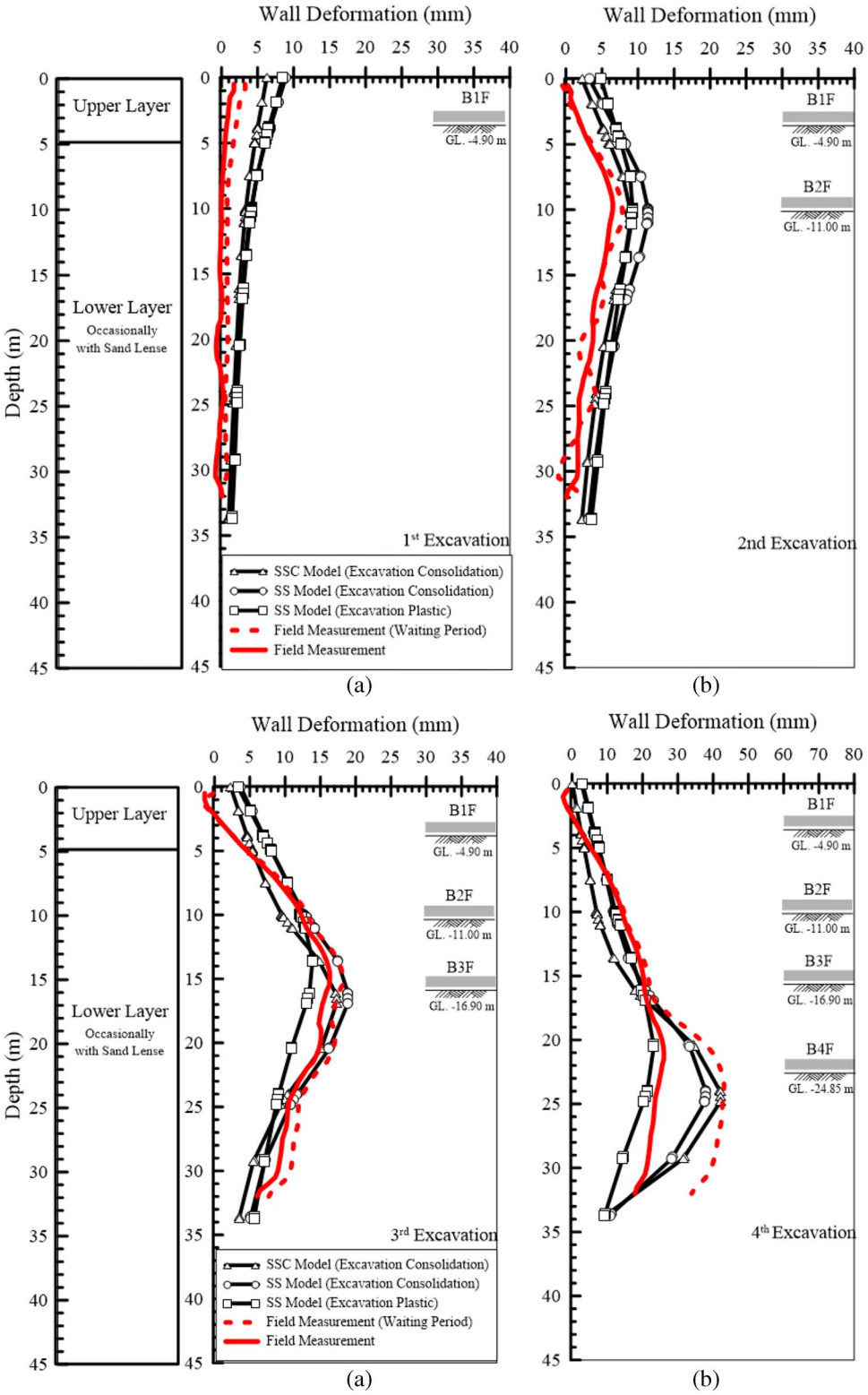

Fig. 18 Wall deformation results obtained using the SSC model (with sand lenses added) for the no-embankment side

after slab completion in the final stage. For both sides, the maximum wall deflection obtained in the simulation was 44.7 mm. Moreover, the field measurement for the maximum wall displacement 1 month after the completion of the slab was 43.1 mm at the no-embankment side and 46.3 mm at the embankment side. Theoretically, the presence of a sand lens accelerates the dissipation of pore water pressure. This increases the effective stress as well as the wall deformation.

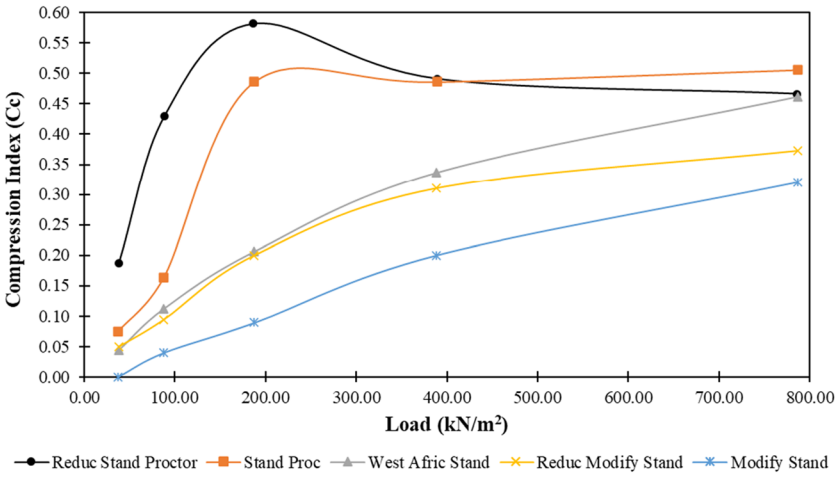

Fig. 19 The impact from loaded used in the oedometer test on compression index (C_c) (Aila 2016)

Table 9 Summary of creep index (C_α) of clays (Zhu et al. 2016)

Clay	Depth/m	C_α	e_0	G_s	w_L	I_P
HKMC	Seabed	0.0054 – 0.0163	1.5	2.66	60	32
Shanghai Clay	12	0.0062 – 0.0076	1.06	2.7	42.5	20
Zhoushan Clay	8	0.0058 – 0.0076	1.07	2.72	40.7	20
Kaolin	-	0.0058 – 0.0062	1.13	2.65	40	20

Discussion

Selections of soil parameters λ^*, κ^* and μ^* are discussed first. As described in Eqs. 1, 2, and 3, these parameters were interpreted from soil parameters C_c, C_s and C_α which were obtained from laboratory tests, such as oedometer tests. That is the reason in this study, these parameters were determined from the laboratory tests at the beginning. However, it is understood though the 1st set parameters (0.1039 & 0.04647 of λ^* and 0.02772 & 0.003319 of κ^*) fit laboratory test data well but the other set parameters (0.05197 & 0.01859 of λ^* and 0.01039 & 0.002655 of κ^*) were chosen to fit later wall displacements and this is unlikely to be consistent with previous statement. More explanations thus have to be undertaken herein.

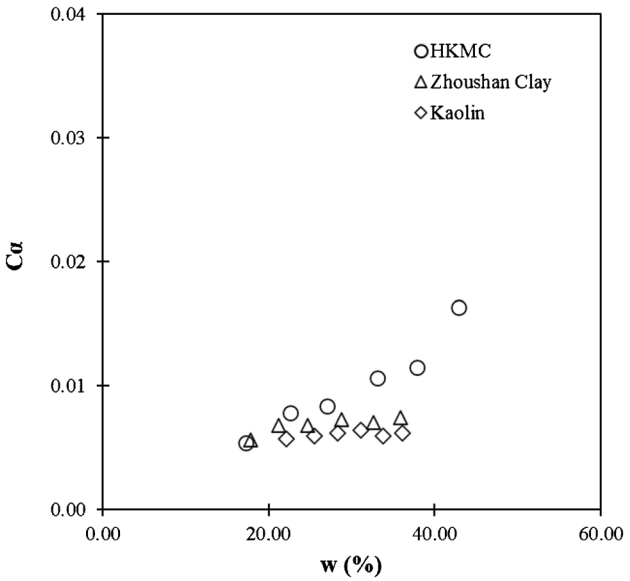

Fig. 20 Variances of C_α from similar clays (Agung 2019)

For λ^* and κ^*, in theory, it should be decided based on laboratory tests but limited samples were taken to carry out tests so results may not be able to provide a full view of soil properties. Further, Aila (Aila 2016) indicated the impact from sample disturbance on results from laboratory tests are significantly and the quality of soil samples could be various in a wide range associated with volume change during the testing. Moreover, as shown in Fig. 19, it is clear the load used in the oedometer test could change results of compression index a lot. Uncertainties stated above could lead to the difference in parameters interpreted from laboratory test results.

By contrast, the authors were involved frequently with field work of the construction which gave more confidence on the monitoring data used in this study. This is expected to be the main reason to decide to accept the other set parameters from feedback analyses of field observations. The interpreted C_c and C_s from adjusted λ^* and κ^* is in the range of 0.11 to 0.30 and 0.02 to 0.11, respectively. Agung (Agung 2019) collected data from similar clays and showed C_c is in the range of 0.03 to 0.82 and C_s is in the range of 0.006 to 0.11. Updated values of C_c and C_s are both within the ranges above so it further approves the reliability of adjusted λ^* and κ^*. Actually, back analyses

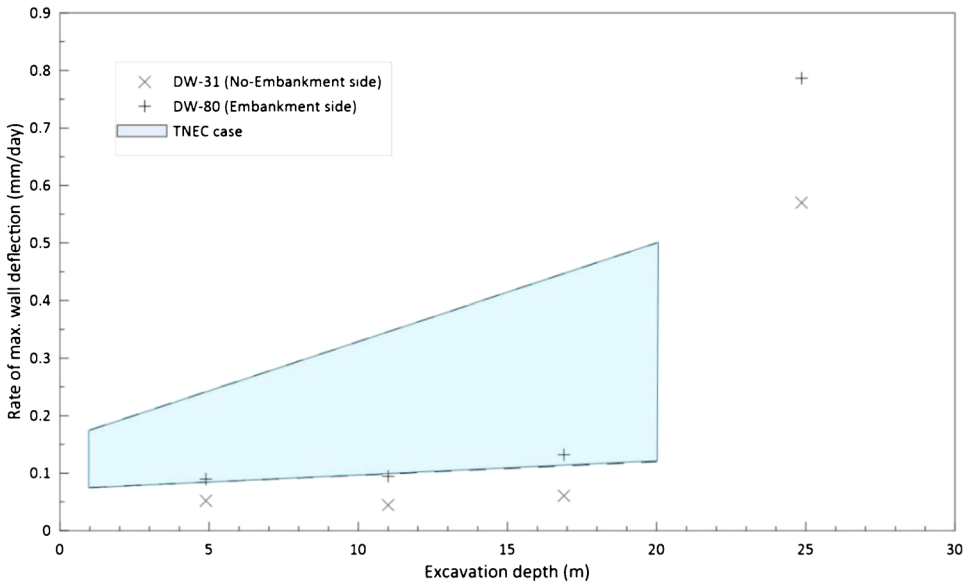

Fig. 21 Rate of maximum wall deflection versus excavation depth

of original parameters used perfectly fit results of oedometer tests but could not completely fulfill data from tri-axial texts. This inconsistence might be also connected with various quality of testing samples and procedures. It is thus suggested too that current sampling and laboratory testing technologies and procedures in Jakarta deserve a space to be improved.

As presented in Eq. 3, μ^* is defined by modified creep index C_α but unfortunately, the test results of C_α is not available for Jakarta clay so C_α from similar clays are collected as an alternative solution. Details of chemical properties of clay at Case A and Case B are reviewed and two main components of seawater, sulfates and chlorides varies in the range of 4 to 550 mg/kg and 16 to 248 mg/kg, respectively. This indicates seawater intrusion has affected soils at Case A and Case B so clays under identical conditions are chosen as references to evaluate C_α and μ^*.

Table 9 presents clays chosen with certain soil properties, such as initial void ratio (e_0), specific gravity (G_s) specific gravity, liquid limit (w_L) and plasticity index (I_P) and Fig. 20 shows C_α is from 0.005 to 0.02 which is consistent with C_α used in this study (Zhu et al. 2016). Comparing with C_α of other clays, seawater might significantly reduce the value.

Observations of lateral wall displacements in the final stage of excavation were compared for Cases A and B, and the excavation-induced displacements were generally larger in Case A than in Case B. This was because of the greater excavation depth and longer waiting period during construction of the floor slab in Case A. Figure 21 shows a plot of the maximum wall deflection rate versus the excavation depth for Case A. This rate was higher during the final stage than the other stages, presumably due to soil creep and the pore water pressure being increasingly dissipated because of the presence of a local sand layer.

The prediction obtained by increasing the permeability of clay and performing consolidation analyses was concluded to be better than the prediction obtained using the function of soil creep in terms of lateral wall displacement in the final excavation stage. This is likely to be inconsistent with what was found by Harahap and Ou (Harahap and Ou 2020), and some reasons can be offered for the difference. First, especially for a large-scale excavation, the slab used in the top-down method is cast zone by zone. Although the waiting period is defined as the time from initiation until full slab completion, certain zones of the slab are expected to form stiff supports in advance, particularly for a comparatively narrow excavation, despite the slab not being completely finished; these stiff supports may help to reduce the displacement induced by the creep of clay. Moreover, Hsiung (Hsiung 2002) indicated that the pore pressure remains the same or slightly rises at the end of each excavation stage in soft clay in Taipei but dramatically increases for excavations in Gault clay, which is stiff clay found in the United Kingdom. In conjunction with any drained material, such as a sand lens in the ground, the consolidation of stiff clay may lead to additional displacement; this may help explain the extremely large lateral wall displacement of Section D-D in Case B, in addition to the impact of the opening of the floor slab (Hsiung et al. 2018). Finally, soft clay was much thicker in the case in Taipei (Harahap and Ou 2020) than in the cases in Bangkok (Likitlersuang et al. 2013) and Central Jakarta (Hsiung et al. 2018); thus, the accumulated displacement caused by soil creep was likely closely connected to the thickness of the soft clay. Furthermore, the soft clay was thinner in both Case A and Case B, and soil creep is thus anticipated to have played a much less crucial role than that played by consolidation in the time-dependent behavior of the excavations; therefore, the change in the creep index should not have had a major impact. Laboratory test data on creep are not available to validate this speculation, however.

Conclusion

This paper presents numerical analyses of two large-scale and well-documented deep excavations that were made in Central Jakarta. The soil parameters, geotechnical characteristics, and time-dependent behavior of excavations were examined through 3D FE analyses. The following were the major conclusions:

1. The soft-soil model was employed to analyze the geotechnical characteristics in Central Jakarta, and it performed well for both cases. This model can be used as a reference when considering those variables.
2. The time-dependent characteristics of soils were discovered to contribute up to 23%–26% to the total wall deflection.
3. When a sand lens was added to the soft soil creep model, the model's results were found to agree favorably with the field measurements made approximately 1 month after the completion of the slab. This confirmed that both soil creep and dissipation of excess pore water pressure played a role in the large wall deformation in the final stage for Case A, but consolidation caused by the excavation played a more major role than the creep of soil did. These results may be connected to the zone casting of a comparatively narrow excavation, generation of excess pore pressure with or without drained materials (such as sand lenses), and the thickness of the soft clay.

Acknowledgements The authors would like to thank to all personnel and parties involved in both field and laboratory test works as well as providing necessary data for two case histories used in this paper.

Data Availability Due to contractual/commercial restrictions, supporting data for this research is not available.

Declarations

Conflicts of interests/Competing interests The authors declare no conflict of interest.

References

Agung MD (2019) Three- dimensional numerical analysis on excavation in Central Jakarta with consideration of time-dependent soil behaviour, MSc thesis, National Taiwan University of Science and Technology, Taiwan

Aila W (2016) Establishment of geotechnical properties and 3D numerical model for deep excavation in Central Jakarta, MSc thesis, National Taiwan University of Science and Technology, Taiwan

Bakr M (2015) Influence of Groundwater Management on Land Subsidence in Deltas. Water Resour Manag 29(5):1541–1555. https://doi.org/10.1007/s11269-014-0893-7

Brinkgreve R, Engin E, Swolfs WJR (2017) Plaxis manual. Balkema, Netherlands

Clough GW, Q'Rourke TD (1990) Construction-induced movements of in situ walls. Design and performance of earth retaining structures. ASCE Spec Publ 25:439–470

Dong Y, Burd HJ, Houlsby GT (2017) Finite element study of deep excavation construction processes. Soils Found 57(6):965–979. https://doi.org/10.1016/j.sandf.2017.08.024

Edil TB, Benson CH, Li L, Mickelson D, Camargo FF (2009) Comparison of Basic Laboratory Test Results with More Sophisticated Laboratory and In-situ Tests Methods on Soils In Southeastern Wisconsin. University of Wisconsin-Madison

Finno RJ, Arboleda-Monsalve LG, Sarabia F (2015) Observed performance of the One Museum park west excavation. J Geotech Geoenviron Eng 141(1):04014078. https://doi.org/10.1061/(ASCE)GT.1943-5606.0001187

Firmansyah I, Sukamta D (2000) Common Practice Basement Construction in Jakarta-Indonesia. ACF Symposium Tech Rep 28–39

Harahap SE, Ou CY (2020) Finite element analysis of time-dependent behavior in deep excavations. Comput Geotech 119:103300. https://doi.org/10.1016/j.compgeo.2019.103300

Hsiung BCB (2002) Engineering performance of deep excavation in Taipei. PhD thesis, University of Bristol, UK

Hsiung BCB, Yang KH, Aila W, Ge L (2018) Evaluation of the wall deflections of a deep excavation in Central Jakarta using three-dimensional modeling. Tunn Undergr Space Technol 72:84–96. https://doi.org/10.1016/j.tust.2017.11.013

Kooi H, Erkens G (2020) Creep consolidation in land subsidence modelling; integrating geotechnical and hydrological approaches in a new MODFLOW package (SUB-CR). Proc Int Assoc Hydrol Sci 382:499–503. https://doi.org/10.5194/piahs-382-499-2020

Likitlersuang S, Surarak C, Wanatowski D, Oh E, Balasubramaniam A (2013) Finite element analysis of a deep excavation: A case study from Bangkok MRT. Soil Found 53(5):756–773. https://doi.org/10.1016/j.sandf.2013.08.013

Lin HD (1992) Soil creep and deep excavation. Sino- Geotechnics 40:25–34 (in Chinese)

Lin HD, Ou CY, Wang CC (2002) Time-dependent displacement of diaphragm wall induced by soil creep. J Chin Inst Eng 25(2):223–231. https://doi.org/10.1080/02533839.2002.9670697

Lin HD, Wang CC (1995) Creep effects on deformation of deep excavation. 10th Asian Regional Conference on Soil Mechanics and Foundation Engineering, Beijing, China, Volume 1:321- 324

Ou CY, Chiou DC, Wu TS (1996) Three-dimensional finite element analysis of deep excavations. J Geotech Eng 122(5):337–345. https://doi.org/10.1061/(ASCE)0733-9410(1996)122:5(337)

Ou CY, Liao JT, Lin HD (1998) Performance of diaphragm wall constructed using top-down method. J Geotech Geoenviron Eng 124(9):798–808. https://doi.org/10.1061/(ASCE)1090-0241(1998)124:9(798)

Ou CY (2006) Deep excavation: theory and practice. CRC Press, London, UK

Peck RB (1969) Deep excavation and tunneling in soft ground. State-of-the-Art Report. In: Proceedings of the 7th International Conference on Soil Mechanics and Foundation Engineering. SMFE, Mexico, pp 225–290

Terzaghi K, Peck RB, Mesri G (1996) Soil mechanics in engineering practice, 3rd edition, Wiley- Interscience

Wu TH, Elrefai ANAA, Hsu IR (1978) Creep deformation of clays. J Geotech Eng Div, ASCE 104(GT1):61–76

Younger JS, Cook JR (1994) The Impact of Characteristics of Indonesian Tropical Soils on Construction. In Proceedings of The International Conference on Soil Mechanics And Foundation Engineering-International Society For Soil Mechanics And Foundation Engineering 4:1493–1493

Yu HD, Chen WZ, Gong Z, Tan XJ, Ma YS, Li XI, Sillen X (2015) Creep behavior of boom clay. Int J Rock Mech Min Sci 76:256–264

Zhu QY, Yin ZY, Hicher PY, Shen SL (2016) Nonlinearity of one-dimensional creep characteristics of soft clays. Acta Geotechnics 11:887–900. https://doi.org/10.1007/s11440-015-0411-y